Appl Nanosci (2016) 6:629–639
DOI 10.1007/s13204-015-0480-0

ORIGINAL ARTICLE

Effects on structural, optical, and magnetic properties of pure and Sr-substituted $MgFe_2O_4$ nanoparticles at different calcination temperatures

A. Loganathan[1] · K. Kumar[2]

Received: 4 March 2015 / Accepted: 2 July 2015 / Published online: 22 July 2015

Abstract In the present work, pure and Sr^{2+} ions substituted Mg ferrite nanoparticles (NPs) had been prepared by co-precipitation method and their structural, optical, and magnetic properties at different calcination temperatures were studied. On this purpose, thermo gravimetric and differential thermal analysis (TG–DTA), Fourier transform infrared spectroscopy (FT-IR), X-ray diffraction (XRD), scanning electron microscopy, UV–Visible diffused reflectance spectroscopy, impedance spectroscopy, and vibrating sample magnetometer were carried out. The exo- and endothermic processes of synthesized precursors were investigated by TG–DTA measurements. The structural properties of the obtained products were examined by XRD analysis and show that the synthesized NPs are in the cubic spinel structure. The existence of two bands around 578–583 and 430–436 cm^{-1} in FT-IR spectrum also confirmed the formation of spinel-structured ferrite NPs. The lattice constants and particle size are estimated using XRD data and found to be strongly dependent on calcination temperatures. The optical, electrical, and magnetic properties of ferrite compositions also investigated and found to be strongly dependant on calcination temperatures.

Keywords Magnetic ferrites · Impedance spectroscopy · VSM

✉ A. Loganathan
aloganathan64@gmail.com

[1] Engineering Physics Section, Annamalai University, Annamalai Nagar, Chidambaram, Tamil Nadu 608 002, India

[2] Department of Physics, Annamalai University, Annamalai Nagar, Chidambaram, Tamil Nadu 608 002, India

Introduction

In the vast application of nanomaterials, the sizes of magnetic and electronic devices are reduced greatly in the recent year. Spinel ferrite nanomaterials are regarded as one of the most important inorganic nanomaterials because of their improved electrical (Rane et al. 2001), magnetic (Kotnala et al. 2009), and catalytic properties (Srivastava et al. 2009), respectively. Their physical and chemical properties of spinel ferrites are different from their corresponding bulk materials due to their higher surface to volume ratio (Naseri et al. 2011). The unit cell of spinel ferrite belongs to the cubic structure, oxygen anions formed the close face-centered cubic (fcc) packing consisting of 64 tetrahedral (A) and 32 octahedral (B) metal ions. In a normal spinel structure, the chemical formula takes in the form of A^{2+} $[B^{3+}]_2$ O_4. From this structure, the A^{2+} cations occupied the tetrahedral site, whereas the B^{3+} cations occupy the octahedral site (Nakagomi et al. 2009). The structural, electrical, chemical, and magnetic properties of metal ferrites strongly depend upon the nature of the ions and their distribution among the A- and B-sites, respectively (Baykal et al. 2008). The introduction of different metallic ions in the spinel structure, alter the distribution of ions in both sites and leads to variations in magnetic and electric properties (Ahmed et al. 2004). And also, the blocking temperature, saturation magnetization, and coercivity are clearly size dependent. So that, the particle size is an important factor to control their property of ferrite nanoparticles (NPs) (Liu and Zhang 2001). Spinel-type ferrites are commonly used in many electronic and magnetic devices due to their high magnetic permeability and low magnetic losses (Giannakopoulou et al. 2002). High electrical resistance and lower saturation magnetization makes them suitable for magnetic and magneto-optical

applications (Kim et al. 2001). Among various ferrite NPs, $MgFe_2O_4$ has special attention in modern material due to their improved electrical and magnetic properties (Chen and Zhang 1998; Zhang et al. 2011).

Several reports are available for the introduction of different metallic ions such as Zn, Cu, Li, and Mn into $MgFe_2O_4$, and their structural, electrical, and magnetic properties were studied well (Bharti et al. 2010; Mansour 2011). However, the effects of Sr^{2+} ions in spinel $MgFe_2O_4$ are not yet reported. The first systematic study in the field of preparing of spinel ferrites was reported by Hilpert in 1909 (Hilpert 1909). Recently, various fabrication methods have been reported, including the sol–gel (Thankachan et al. 2013), co-precipitation (Ferk et al. 2014), solid-state reaction (Kotnala et al. 2008), ball milling (Chen et al. 2012), hydrothermal method (Hemeda et al. 2014; Koseoglu 2013), and combustion technique (Deraz and Shaban 2009) etc. Among these, co-precipitation method is one of the advance methods for preparation of metal ferrite NPs because of its simplicity, low cost, and bulk production of NPs. In this work, a chemical co-precipitation method was used to prepare pure and Sr^{2+} substituted $MgFe_2O_4$ precursors. The obtained precursors were calcinated at different temperatures and their thermal, structural, optical, and magnetic properties were studied by thermo gravimetric and differential thermal (TG and DTA) analyses, X-ray diffraction (XRD), Fourier transform infrared (FT-IR) spectroscopy, scanning electron microscopy (SEM), UV–Visible diffused reflectance spectroscopy (UV–Vis-DRS), Impedance, and vibrating sample magnetometer (VSM) analysis.

Materials and methods

In the present work, the raw materials of magnesium nitrate ($Mg(NO_3)_3{\cdot}6H_2O$), iron nitrate ($Fe(NO_3)_3{\cdot}9H_2O$), strontium nitrate $Sr(NO_3)_2$, and sodium hydroxide (NaOH) were used to prepare pure and Sr^{2+} substituted $MgFe_2O_4$ NPs in co-precipitation method. Deionized water was used as a solvent. All the chemicals have the purity of more than 99 % and are used without further purification.

For synthesis of pure magnesium ferrite NPs, 0.2 mol magnesium nitrate and 0.4 mol iron nitrate were dissolved in 100 mL of deionized water. The resulting solution was stirred under constant stirring at 90 °C on the hot plate, until a clear solution was formed. Further, 6 mol of NaOH was added into a solution and the pH of the solution was kept in the range of 12–13. Finally, the brown color precipitate was formed. The formation of brown color precipitate indicates that metal nitrates were converting into metal hydroxide. The resulting precipitate was stirred for 2 h at a reaction temperature. The obtained precipitates were filtered and washed several times with deionized water for removal of unreacted precursor. Further, the precursor was dried in the electric oven overnight to get the dried powder. This dried precursor powder was divided into three equal parts and calcinated for 3 h at different temperatures (700, 800, and 900 °C respectively). In a similar way, Sr^{2+} substituted magnesium ferrite was synthesized.

Experimental details

The decomposition process of the precursors and formation process of the pure and Sr-substituted $MgFe_2O_4$ NPs are investigated by TG and DTA analyses with heading rate of 20 °C per mints installed at CISL, Annamalai University. The structural and phase formation of ferrite NPs were identified by XRD analysis (X' PERT PRO-PANalytical, PHILIPS) with CuKα ($\lambda = 1.54$ Å) radiation, anode at 40 kV, and current of 30 mA in the range of 20°–80°, available at Department of Physics, Alagappa University, Karaikudi, Tamil Nadu. The obtained peaks were compared with the Joint Committee of Powder Diffraction Standard (JCPDS) files. The functional groups present in the surface of obtained ferrite compositions were investigated by FT-IR measurements performed in transmission mode in the wavenumber range of 4000–400 cm^{-1} by Perkin Elmer Spectrum RXI (FT-IR) spectrometer available at St. Joseph's college, Tiruchy, Tamil Nadu. The two-dimensional surface morphological natures of synthesized samples were carried out by Scanning electron microscope (SEM-JSM-5610 LUJELO model) at different magnifications available at CISL, Annamalai University, Tamil Nadu. For evaluation of optical properties of ferrite compositions, UV–Vis diffuse reflectance spectrums were carried out in the wavelength range of 200–900 nm using UV140404B available at Cochin University, Kerala. Impedance measurements were carried out using versaSTAT MC impedance spectrometer in the frequency range of 1 Hz–1 MHz available at St. Joseph's college, Tiruchy, Tamil Nadu. VSM analysis was performed at room temperature to study the magnetic behavior of ferrite composition on the effect of calcination temperature in Lake Shore-7404 available at Central Instrumentation Facility, Pondicherry, India.

Results and discussion

Thermal analysis

The decomposition process of synthesized precursors and formation process of the pure and Sr^{2+} substituted $MgFe_2O_4$ NPs are investigated by TG and DTA. Figures 1 and 2 shows the TG–DTA results of the obtained product

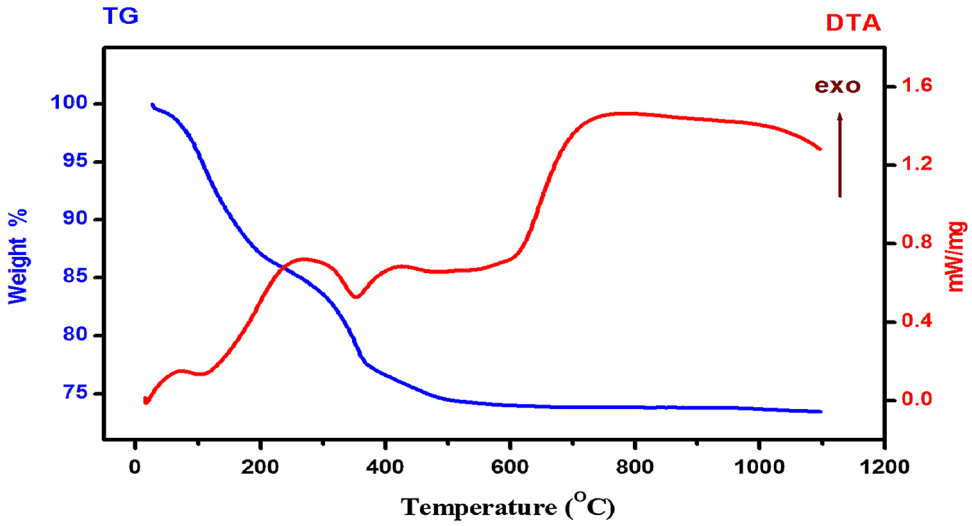

Fig. 1 TG–DTA analysis of pure $MgFe_2O_4$ precursor

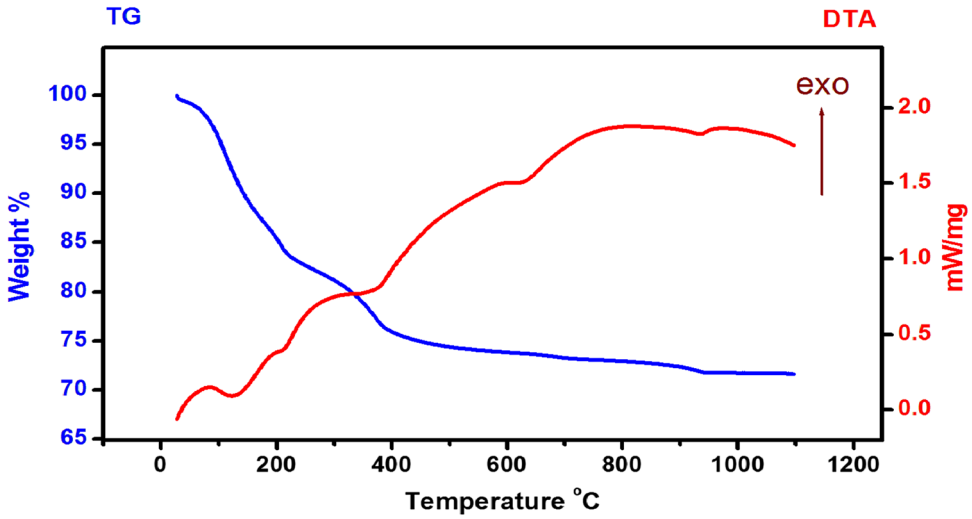

Fig. 2 TG–DTA analysis of Sr^{2+} substituted $MgFe_2O_4$ precursor

of pure and Sr^{2+} substituted magnesium ferrite precursor. From this observation, similar weight losses are observed in both samples. As the temperature is increased from 28 to 1100 °C, the dried precursor lost its overall weight about 26 and 29 % for pure and Sr^{2+} substituted ferrites, respectively. The first weight loss in the TG curve appears in the range of 28–280 °C, due to evaporation of residual water present in the product and shows a corresponding weight loss of 13 %. The next exothermic peak appears in the DTA curve around 430 °C, and TG curve shows the weight loss (9 %) in the temperature range between 210 and 387 °C, which is attributed to the decomposition of organic compounds and transformation of metal hydroxide into metal oxides as given in following equations.

$$Mg\ (OH)_2 \rightarrow\ MgO\ +\ H_2O, \quad (1)$$

$$2Fe\ (OH)_3 \rightarrow\ Fe_2O_3 + 3H_2O, \quad (2)$$

$$Sr\ (OH)_2 \rightarrow\ SrO\ +\ H_2O. \quad (3)$$

After that, gradual change in weight loss is observed up to 630 °C, which is a corresponding weight loss of 3.5 %, attributed to the decomposition of metal oxide into metal ferrite as given in Eqs. (4) and (5).

$$MgO\ +\ Fe_2O_3 \rightarrow\ MgFe_2O_4, \quad (4)$$

$$(MgO)_{1-x} + (SrO)_x + Fe_2O_3 \rightarrow\ Mg_{1-x}Sr_xFe_2O_4. \quad (5)$$

Beyond the temperature 630 °C, no weight loss is observed in both pure and Sr^{2+} substituted $MgFe_2O_4$ precursor. It indicates the formation of stable ferrite in both samples. Further the formations of ferrite NPs are confirmed by XRD results.

Functional analysis (FT-IR)

The FT-IR spectroscopy is used to identify their functional groups present in the ferrite compositions. All the FT-IR characterizations are performed at room temperature in the

wave number range of 4000–400 cm^{-1}. Figures 3 and 4 show the FT-IR spectra of pure and Sr^{2+} substituted $MgFe_2O_4$ ferrite NPs, respectively. The FT-IR spectra shows two strong band assignments in the range below 1000 cm^{-1}, attributable to the band assignment between inorganic elements and oxygen ions (Modi et al. 2013). Normally, the higher frequency band is observed in the range of 600–500 cm^{-1}, corresponds to vibrations of the A-site [$M_{tetra}\leftrightarrow O$] and the lower frequency band observed in the range of 500–400 cm^{-1}, due to the vibrations of the B-site groups [$M_{octa}\leftrightarrow O$]. These two bands are common features for all ferrites (Waldron 1955; Labde et al. 2003). The vibration of band in the tetrahedral sites occurs at higher wavenumber than octahedral sites, which is due to the smaller bond length of tetrahedral positions compared to the octahedral sites (Pradeep et al. 2011). In pure $MgFe_2O_4$ samples, the tetrahedral frequency band v_1 is observed at 579, 580, and 575 cm^{-1} whereas the octahedral frequency band v_2 is observed at 437, 438, and 432 cm^{-1} in the calcination temperatures of 700, 800, and 900 °C, respectively. As shown in Fig. 3b, slight variations of band positions are observed with increasing calcination temperatures. It mainly attributes the variation in ion distribution between tetrahedral and octahedral sites with calcination temperatures. But, in case of Sr^{2+} substituted samples, these bands are shifted to the higher wavenumber range (Fig. 4a, b). The variation in A-site band assignment is higher than B-sites which attributes that the Sr^{2+} ion preference to B-site. Due to the presence of large size Sr^{2+} ions in B-sites, some of the Fe^{2+} ions migrate into A-sites as consequently tetrahedral vibration increases considerably. The peak present at around 1130 cm^{-1} due to stretching vibration of C–O group and stretching of O–H band from the surface water molecules appears at around 3324 cm^{-1}.

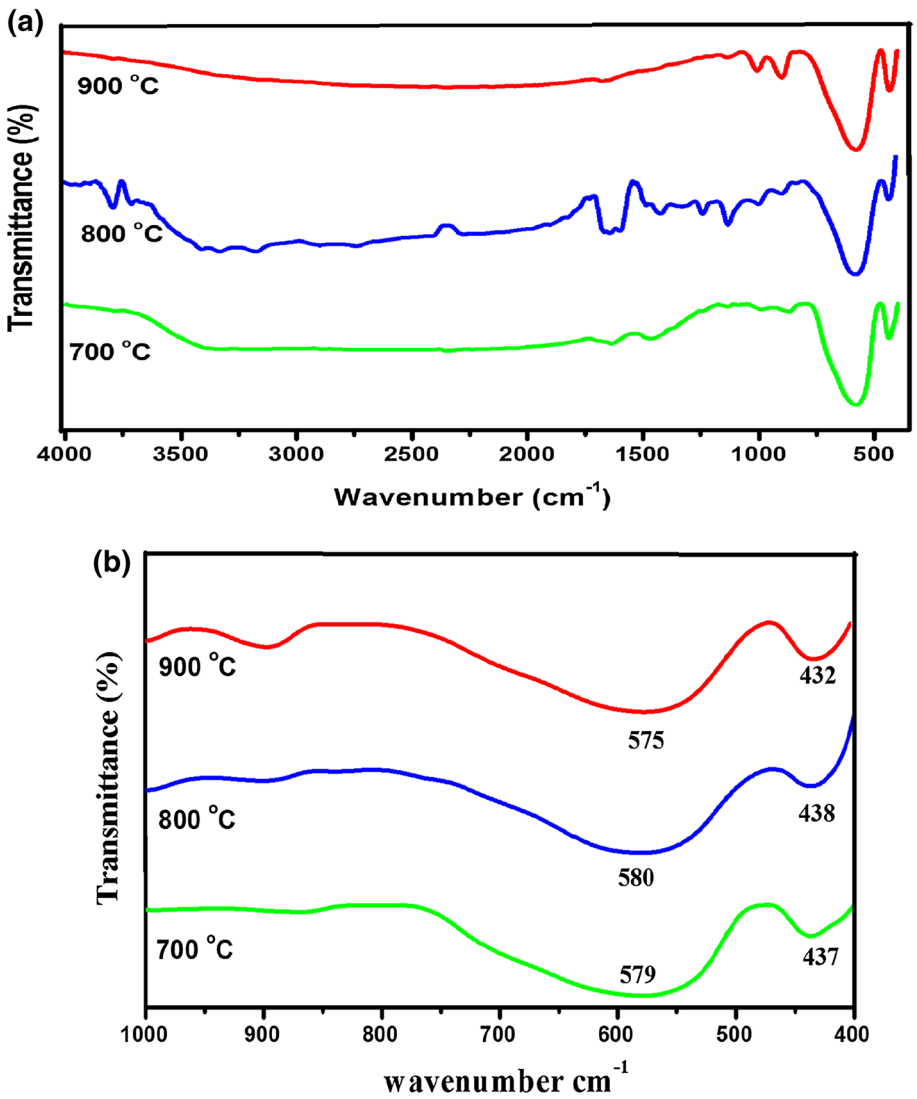

Fig. 3 **a** FT-IR spectra of pure $MgFe_2O_4$ nanoparticles at different calcination temperatures in the wavenumber region of 4000–400 cm^{-1}, **b** selected wavenumber region 1000–400 cm^{-1}

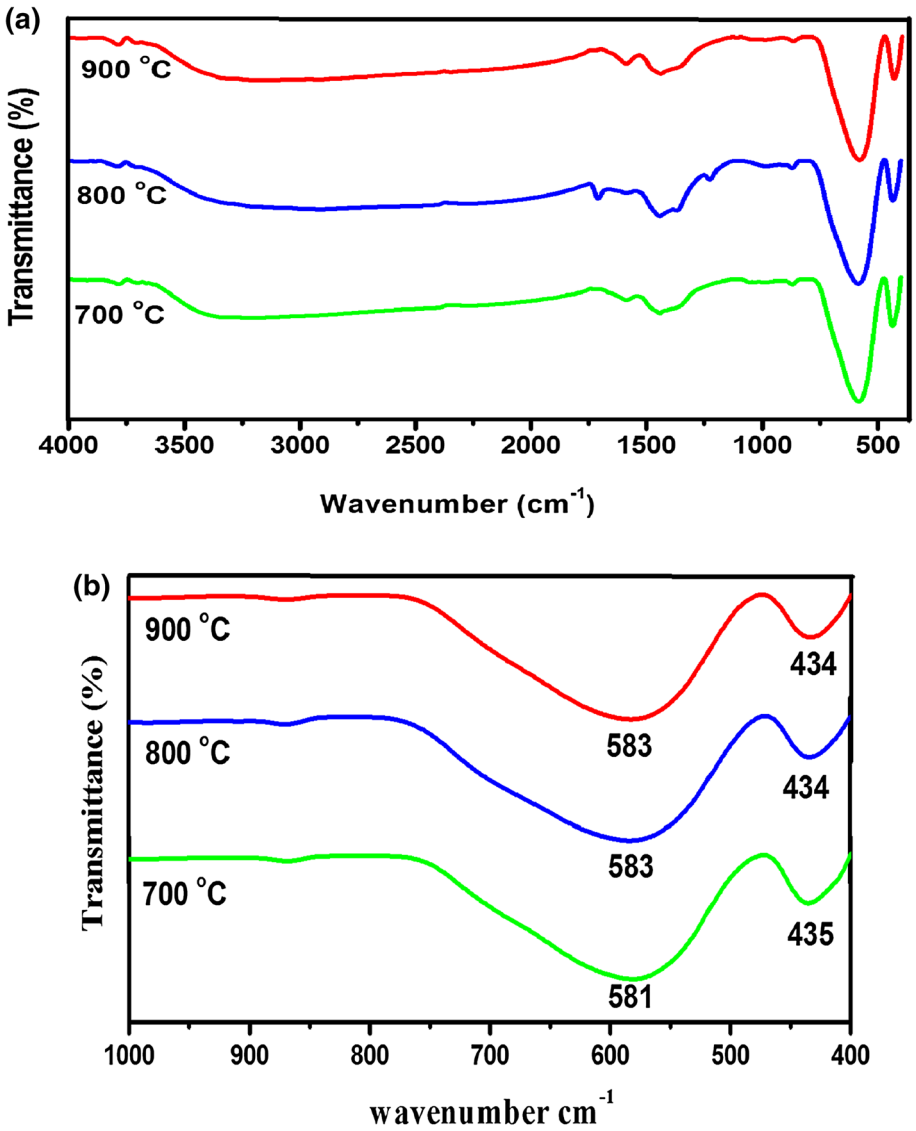

Fig. 4 **a** FT-IR spectra of Sr-doped $MgFe_2O_4$ nanoparticles at different calcination temperatures in the wavenumber region of 4000–400 cm^{-1}, **b** selected wavenumber region 1000–400 cm^{-1}

Structural analysis

To evaluate their structural properties of ferrite NPs, XRD characterization is carried out. Figures 5 and 6 show the XRD pattern of the pure and Sr-substituted $MgFe_2O_4$ NPs obtained at different calcination temperatures. The XRD spectrum obtained at low temperature (700 °C) shows the prominent diffraction peaks of pure magnesium ferrite, appeared in 35.5° corresponding to the diffraction plane of (311) which indicates that formation of $MgFe_2O_4$ (JCPDS file no. 71-1232) and similar results are observed at all the temperatures as shown in Fig. 5. However, small quantity of another phase, such as α-Fe_2O_3 was also observed (shown as x in Fig. 5). When the calcination temperatures are increased (800 and 900 °C), the intensity of diffraction peaks increased and impurities of the products are reduced compared to the results obtained at 700 °C. This observation shows that the calcination temperatures have the significant role in the formation of magnesium ferrites. The XRD spectrum of $MgFe_2O_4$ obtained at 900 °C shows

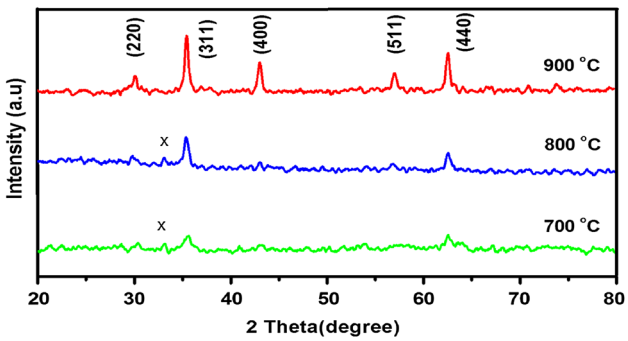

Fig. 5 XRD patterns of pure $MgFe_2O_4$ nanoparticles at different calcination temperatures

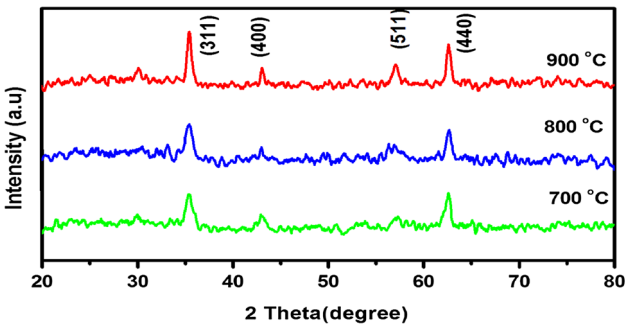

Fig. 6 XRD patterns of Sr^{2+} substituted $MgFe_2O_4$ nanoparticles at different calcination temperatures

high crystalline nature and diffraction peaks (2θ) observed in 30.17°, 35.52°, 43.08°, 57.08°, and 62.64° corresponding to (2 2 0), (3 1 1), (4 0 0), (5 1 1), and (4 4 0) planes, match well again with JCPDS file no 71-1232. In the case of Sr^{2+} substituted $MgFe_2O_4$ NPs, similar results are observed. However, the diffraction angle in (311) plane shifted toward low angle (35.3°) sites. This may be due to the increase in cell volume by an increase in lattice constant by the substitution of Sr^{2+} in the place of Mg^{2+} ions (Toledo et al. 2000). A similar result was reported by Bhukal et al. (2014). From XRD results, the lattice parameters (a) are determined using relation (6).

$$a = d_{hkl}\left[h^2 + k^2 + l^2\right]^{1/2}, \tag{6}$$

where a is the lattice parameter, d is the lattice spacing between two planes, and h, k, l are the miller indices. The average grain size of ferrite compositions is measured by Scherer's formula (Cullity 1956),

$$D = K\lambda/\beta\cos\theta, \tag{7}$$

where λ is the wavelength of the X-ray source used in XRD measurement, β is the peak width of the diffraction peak profile at half maximum in radians, normally highest values of β result in the small grain size, K is called shape factor, which usually takes a value of about 0.9. The lattice parameters are found to be in the range of 8.37–8.39 and 8.39–8.42 Å for pure and Sr^{2+} substituted NPs, respectively as shown in Table 1. The variation of lattice parameters in different calcination temperatures implies that the variation in the ion distribution between both A and B sides. But in the case of Sr^{2+} substituted ferrite NPs, The lattice parameters are found to be higher than the pure magnesium ferrite NPs. It is due to the larger ionic radius, Sr^{2+} (1.27 Å) cation replaced in the place of Mg^{2+} (0.72 Å) in the spinel structure. The grain size of both pure and Sr^{2+} substituted NPs are estimated using the Debye–Scherrer equation and is found to be increased with the calcination temperature lying in the range between 8–30 and 8–24 nm, respectively. At the same calcination temperatures, the crystallite size obtained in Sr^{2+} substituted $MgFe_2O_4$ was found to be lower compared to pure $MgFe_2O_4$ NPs. These results conclude that the Sr^{2+} ions restrict the grain growth of the ferrite phase, whereas calcination temperatures engage their grain growth. The crystallite size less than 50 nm is desirable for obtaining a suitable signal-to-noise ratio for switching applications (Mahmood et al. 2013).

Morphological analysis

The SEM characterization is used to identify their microstructure nature of ferrite NPs. Figure 7 shows the two-dimensional surface morphological images of pure and Sr^{2+} substituted $MgFe_2O_4$ NPs obtained at 900 °C. Figures 7a, b reveal the SEM images of pure $MgFe_2O_4$ ferrite NPs, which show the highly agglomerated spherical-shaped particles. The agglomeration of pure $MgFe_2O_4$ ferrite NPs may arise from magnetic interactions between ferrite particles. On the other hand, the Sr^{2+} substituted $MgFe_2O_4$ ferrite shows the uniform distribution of spherical-shaped particles with moderate agglomeration on Fig. 7c, d.

Optical study (UV–Vis-DRS)

The optical properties of pure and strontium-substituted ferrite NPs are investigated by UV–Vis-DRS spectroscopy. Figures 8 and 9 depict the reflectance spectra of pure and Sr^{2+} substituted magnesium ferrite NPs in the spectral range of 300–900 nm, respectively. It is clear that all the samples show optical properties in the visible region. In pure $MgFe_2O_4$ samples, reflectance percentage decreases with increasing calcination temperatures, but in case of Sr^{2+} substituted samples reflectance percentage increased with increasing calcination temperatures. The decreasing trend of reflectance values in pure magnesium ferrite can be explained by densification of structure with an increase in calcination temperatures. The increasing behavior of reflectance values in Sr^{2+} substituted samples due to the presence of defect in the crystal lattice by agreement with XRD results. The band gap energy of synthesized samples derived from the optical reflectance data using Kubelka–Munk function F(R) (Manikandan et al. 2013),

$$\mathrm{F}(R) = (1-R)^2/2R, \tag{8}$$

where R is the diffuse reflectance. The band gap values of synthesized products are estimated by the graph plotted between $[\mathrm{F}(R)\,h\nu]^2$ versus $h\nu$ (Figs. 10, 11). The estimated values of band gap for pure and Sr^{2+} substituted samples are 2.1, 2, 1.9 and 2.1, 1.8, 1.7 eV, respectively. From this observation, the band gap energy decreases with increasing

Table 1 The structural parameter of pure and Sr^{2+} substituted $MgFe_2O_4$ ferrite nanoparticles

	Temperature (°C)	2θ (°)	d_{hkl} (Å)	a (Å)	V (Å^3)	D (nm)
$MgFe_2O_4$	700	35.5	2.526	8.377	587.86	8
	800	35.43	2.531	8.3943	591.85	21
	900	35.52	2.525	8.374	587.21	30
$Mg_{0.8}Sr_{0.2}Fe_2O_4$	700	35.3	2.533	8.421	597.16	8
	800	35.43	2.531	8.395	591.64	12
	900	35.3	2.532	8.398	592.28	24

2θ diffraction angle in (311) plane, d_{hkl} spacing, a lattice constant, V volume of the formula unit, D grain size

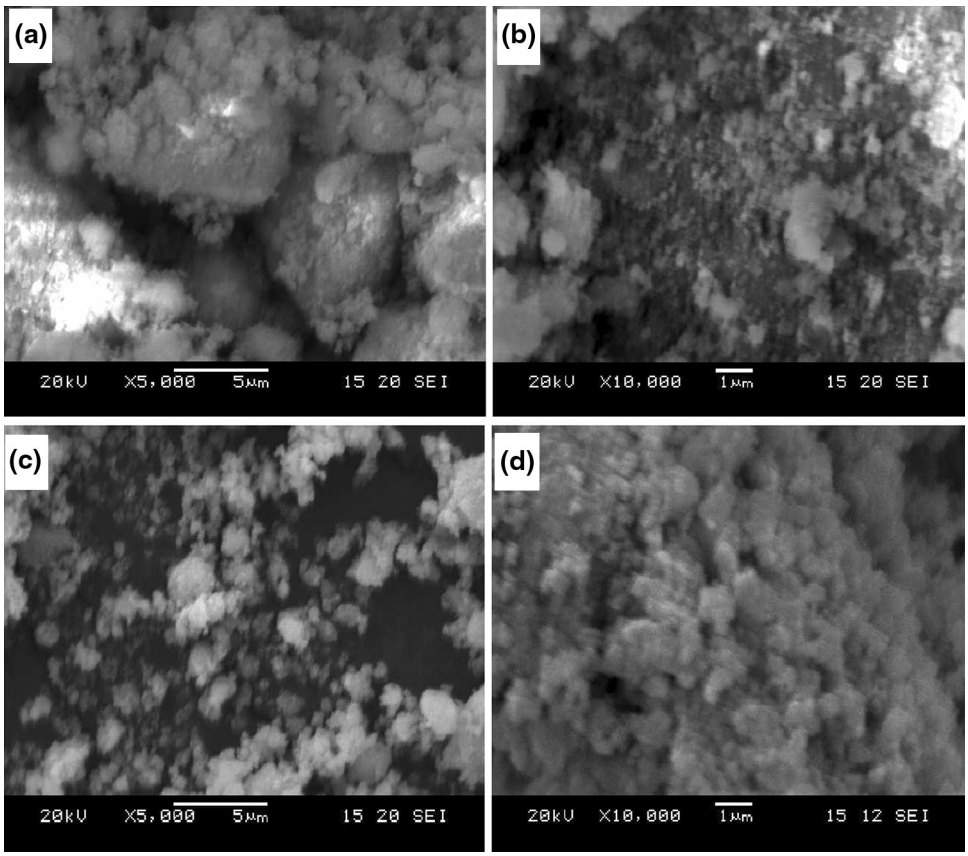

Fig. 7 SEM micrographs of pure $MgFe_2O_4$ (**a**, **b**) and Sr^{2+} substituted $MgFe_2O_4$ (**c**, **d**), respectively

calcination temperatures in both pure and Sr^{2+} substituted samples. The reduction of band gap energy with increasing calcination temperatures probably attribute to the crystallite growth of synthesized product (Roduner 2006).

Impedance analysis

The conductivity of ferrite materials is mainly attributed to the companied effects of bulk or grain and grain boundary contribution. The grain and grain boundary contribution have different relaxation time, which can be separated out by impedance measurement. The complex impedance spectra give the information about the resistive (real part) and reactive (imaginary part) components of a material obtained by plotting the imaginary part of impedance against real part of impedance which is referred to as Nyquist plot, as shown in Figs. 12 and 13 for pure and Sr^{2+} substituted $MgFe_2O_4$ NPs, respectively. All the samples exhibit one semicircle in higher frequency sites and one straight line at low frequency sites depending upon the electrical properties of the materials. The semicircle obtained at high frequency sites represents the resistance of grain and straight line obtained at a low frequency site, represents the resistance of the grain boundary. The obtained results are in good agreement with previous studies (Baruwati et al. 2007; Kotnala et al. 2010). The

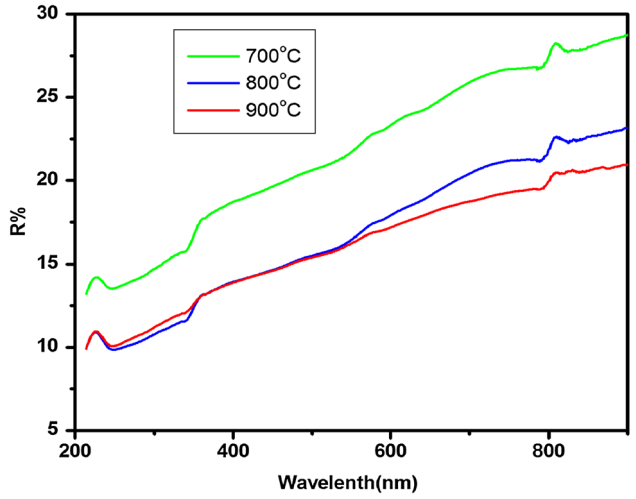

Fig. 8 Reflectance spectra of pure $MgFe_2O_4$ nanoparticles at different calcination temperatures

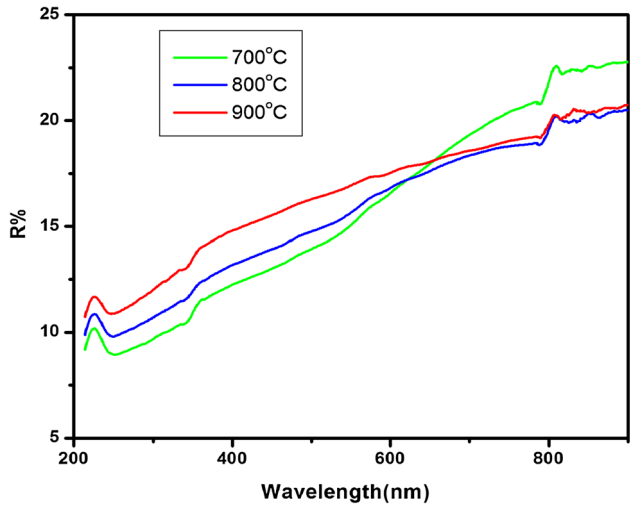

Fig. 9 Reflectance spectra of Sr^{2+} substituted $MgFe_2O_4$ nanoparticles at different calcination temperatures

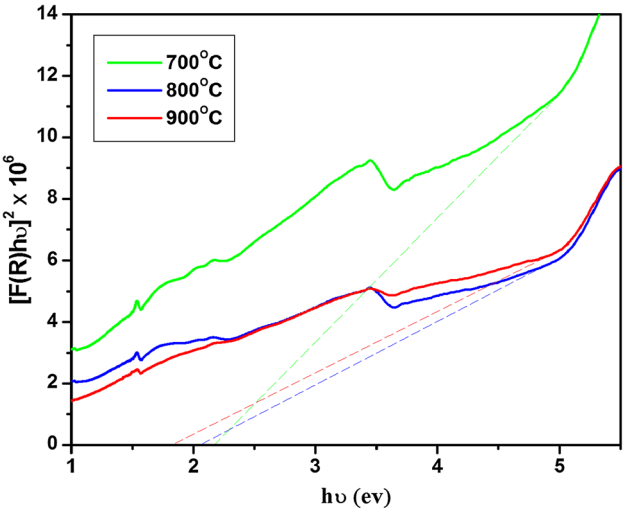

Fig. 10 Band gap energy of pure $MgFe_2O_4$ nanoparticles

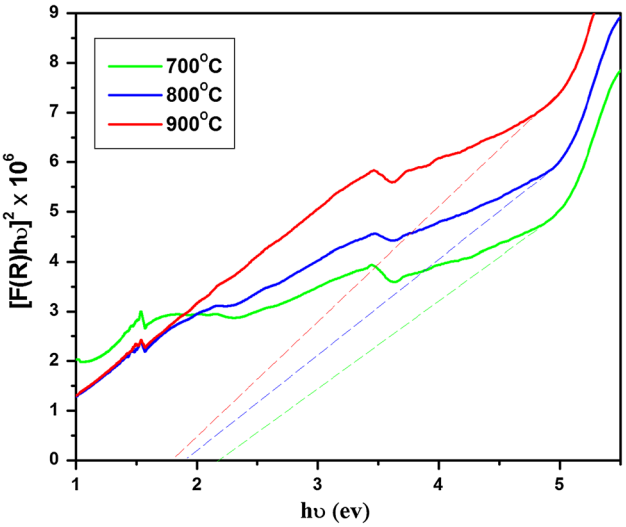

Fig. 11 Band gap energy of Sr substituted $MgFe_2O_4$ nanoparticles

grain resistance plays an important role in the conductivity behavior of the materials and it is much smaller than the grain boundary resistance. The grain resistance of the samples is equal to the diameter of semicircle in Nyquist plot (Ye et al. 2003). In pure $MgFe_2O_4$ sample the diameter of semicircle was increased with calcination temperatures due to the improvement in grain growth with calcination temperatures, whereas its decreases with calcination temperatures in Sr^{2+} substituted samples. The relaxation time and grain capacitance of synthesized samples were estimated using the relation (8),

$$\tau_g = 1/\omega_g = C_g R_g. \quad (9)$$

The obtained values are listed in Table 2. From this observation, calcination temperatures are found to be significant key factors to monitor the conduction process of synthesized samples. The decreasing trend of impedance values in Sr^{2+} substituted samples compared to pure samples, indicate an increase in AC conductivity.

Magnetic study (VSM)

Figure 14a, b depict the room temperature magnetic hysteresis loops for pure and Sr^{2+} substituted magnesium ferrite NPs at different calcination temperatures with a maximum applied field of 12 kOe. The magnetic parameters such as saturation magnetization (M_s), coercive fields (H_c), and magnetocrystalline anisotropy (K) constant are calculated from the hysteresis data and are listed in Table 3. In the present work, the M_s of both NPs are

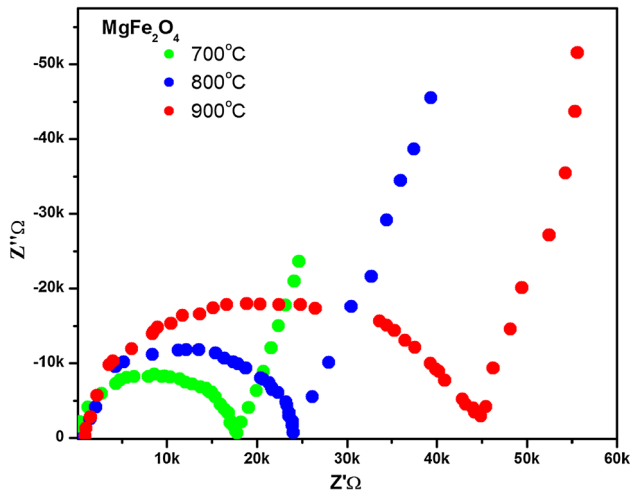

Fig. 12 The Nyquist plot of pure magnesium ferrite nanoparticles at different calcination temperatures

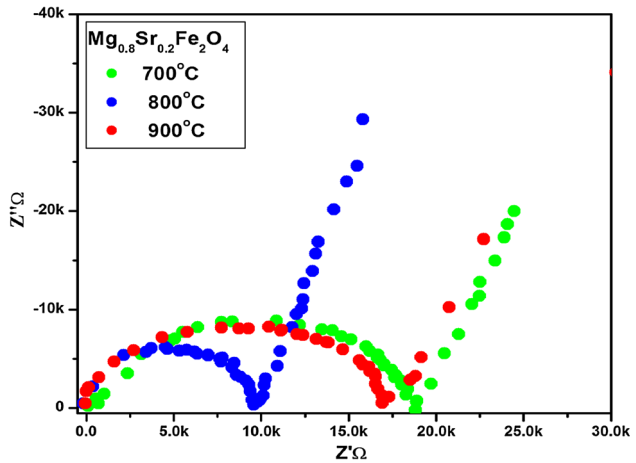

Fig. 13 The Nyquist plot of Sr^{2+} substituted magnesium ferrite nanoparticles at different calcination temperatures

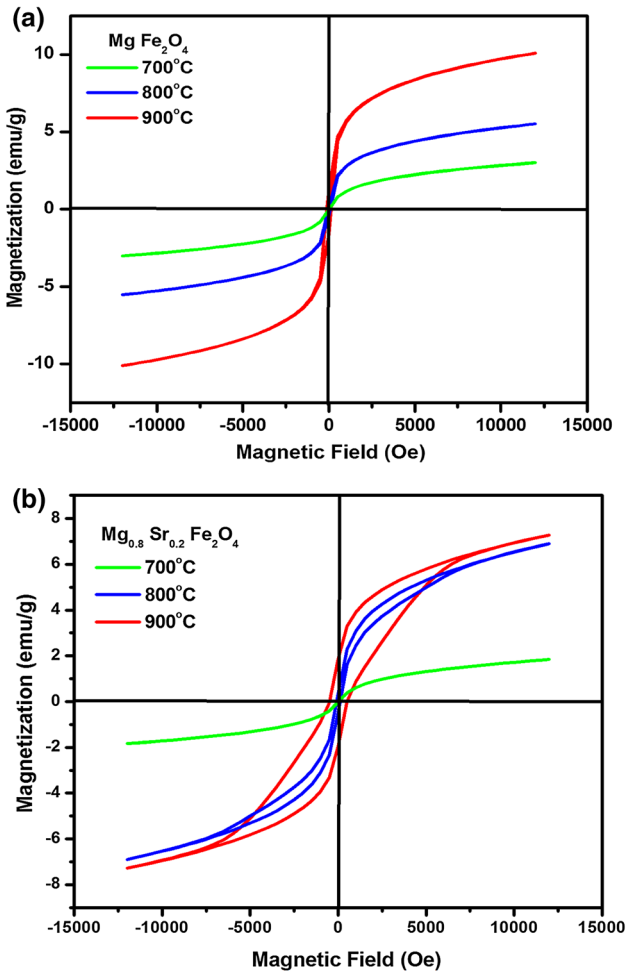

Fig. 14 VSM hysteresis loop of pure (**a**) and Sr^{2+} ions substituted $MgFe_2O_4$ (**b**) nanoparticles calcinated at various temperatures

increased with increasing calcination temperatures in the range between 1.04–10.09 and 1.83–7.27 emu/g for pure and Sr^{2+} substituted NPs, respectively which is smaller than that of bulk magnesium ferrite (about 26.9 emu/g) (Liu et al. 2003). The increasing trend of M_s in both samples might be explained by two factors. The first one is grain size, which increased with calcination temperatures. The sample calcinated at 900 °C, which has a higher grain size, showed higher M_s compared to the other samples. Hence in Sr^{2+} substituted samples, the saturation magnetization values are smaller compared to pure samples at the same calcination temperatures. Compared to pure magnesium ferrite, Sr^{2+} substituted magnesium ferrite has small

Table 2 The impedance parameters of pure and Sr^{2+} ions substituted ferrite nanoparticles measured at room temperature

	T (°C)	τ_g (μs)	R_g (kΩ)	C_g (ÅF)
$MgFe_2O_4$	700	3.4819	17,830	1.9527
	800	3.6460	24,060	1.5154
	900	4.8064	45,964	2.5523
$Mg_{0.8}Sr_{0.2}Fe_2O_4$	700	3.3252	18,830	1.7658
	800	2.7651	9980	2.7713
	900	3.3252	17,660	1.8831

T temperature, τ_g relaxation times, R_g grain resistance, C_g grain capacitance

Table 3 The magnetic parameters of pure and Sr $MgFe_2O_4$ ferrite nanoparticles measured at room temperature

	Temperature (°C)	D (nm)	M_s (emu/g)	H_c (Oe)	K (erg/g)
$MgFe_2O_4$	700	8	1.04	4.47	4.94
	800	21	5.51	59.37	333.80
	900	30	10.09	123.57	1272.26
$Mg_{0.8}Sr_{0.2}Fe_2O_4$	700	8	1.83	5.12	9.56
	800	12	6.89	98.62	693.35
	900	24	7.27	491.69	3647.53

D grain size, M_s saturation magnetization, H_c coercive field, K magnetocrystalline anisotropy constant

grain size at the same calcination temperatures and shows less magnetization values. The other factors can be explained by cation distribution between the tetrahedral and octahedral sites by Neel's sub-lattice collinear model (Néel 1950). According to this model, the saturation magnetization is the vector sum of the magnetic moments of the individual A and B sublattices as for relation $M_s = M_B - M_A$, where M_s is the saturation magnetization, M_B and M_A are the magnetization of B- and A-sites, respectively. In the present study, the synthesized NPs are considered as inverse spinel structure and their cation distribution is estimated as follows.

$$\left(Fe^{3+}_{1-x}Mg^{2+}_{x}\right)_A\left[Mg^{2+}_{1-x}Fe^{3+}_{1+x}\right]_B O_4,$$

$$\left(Fe^{3+}_{1-x}Mg^{2+}_{x}\right)_A\left[Mg^{2+}_{1-x}Sr^{2+}_{0.2}Fe^{3+}_{1+x}\right]_B O_4.$$

It is well known that the Mg^{2+} (0 μ_B) is non-magnetic and Fe^{3+} (5 μ_B) has higher magnetic moment in nature. In inverse spinel, Fe^{3+} ions favor for both tetrahedral and octahedral sites, respectively. When the calcination temperatures increase, ion distribution between A- and B-sites are also modified as follows: in pure magnesium ferrite NPs, part of the Fe^{3+} ions present in A-site migrate to B-site and push some non-magnetic Mg^{2+} to A-site. As a result, magnetic ions in octahedral side increases considerably and lead to increased saturation. In addition, the saturation magnetization of Sr^{2+} substituted ferrite NPs is observed with increase in calcination temperature. However, it is smaller than pure NPs obtained at same calcination temperature. This may be due to the Sr^{2+} ions present in the B-site and the reduced migration of Fe^{3+} ions from tetrahedral side.

The coercivity (H_c) is the magnetic field required for overcoming the magnetocrystalline anisotropy to flip the magnetic moments. This magnetocrystalline anisotropy constant (K) is determined through Stoner–Wohlfarth theory using the following relation (Stoner and Wohlfarth 1948)

$$H_C = 0.98\,K/M_S, \tag{10}$$

where K is the anisotropy constant and M_s is the saturation magnetization. Variation of anisotropy constant K with different calcination temperatures is shown in the Table 3. It shows that the anisotropy constant K gradually increases with temperature in both samples and maximum values are observed in Sr^{2+} substituted NPs. The coercivity of both pure and Sr^{2+} substituted $MgFe_2O_4$ NPs are increased with increasing calcination temperatures. The pure $MgFe_2O_4$ NPs, calcinated at various temperatures show narrow hysteresis loop with very small coercivity values, evident for soft magnetic nature of synthesized samples. As compared with pure NPs, Sr^{2+} substituted NPs at 700 °C show a narrow hysteresis loop with small coercivity value belonging to the soft magnetic nature of synthesized NPs. However, when the calcination temperatures are increased to 800 °C, the coercivity values also increase. The maximum value of coercivity 3647 erg/g is observed in ferrite NPs obtained at 900 °C. This indicates that both pure and Sr^{2+} substituted ferrite NPs exhibit ferromagnetic nature.

Conclusions

From the present study, the pure and Sr^{2+} substituted magnesium ferrite NPs were successfully prepared by co-precipitation methods and their structural, morphological, optical, and electrical properties were studied with different calcination temperatures. The lattice constant and grain sizes were found to be increased with the increasing calcination temperatures. FT-IR study revealed the formation of spinel ferrite structure with two strong peaks at around 575–583 and 432–438 cm^{-1}, respectively. Further, the formation of cubic spinel-structured ferrite was confirmed by XRD spectra. The observed band gap values for pure and Sr^{2+} substituted NPs lies in the range of 2.1–1.9 and 2.1–1.7 eV, respectively. The impedance parameters such as grain resistance, grain capacitance, and relaxation time were also calculated and found to be increased with calcination temperatures in pure magnesium ferrite NPs whereas it decreased in Sr^{2+} substituted samples. The VSM analysis confirmed the existence of ferromagnetic nature of Sr^{2+} substituted ferrite NPs. In summary, all the properties of ferrite NPs are strongly influenced by calcination temperatures.

References

Ahmed TT, Rahman IZ, Rahman MA (2004) Study on the properties of the copper substituted NiZn ferrites. J Mater Process Technol 153–154:797–803

Baruwati B, KumarRana R, Manorama SV (2007) Further insights in the conductivity behavior of nanocrystalline Ni Fe_2 O_{4s}. J Appl Phys 101(1):014302–014307

Baykal A, Kasapoglu N, Koseoglu Y, Toprak MS, Bayrakdar H (2008) CTAB-assisted hydrothermal synthesis of $NiFe_2O_4$ and its magnetic characterization. J Alloys Compd 464:514–518

Bharti DC, Mukherjee K, Majumder SB (2010) Wet chemical synthesis and gas sensing properties of magnesium zinc ferrite nano-particles. J Mater Chem Phys 120:509–517

Bhukal S, Bansal S, Singhal S (2014) Magnetic Mn substituted cobalt zinc ferrite systems: structural, electrical and magnetic properties and their role in photo-catalytic degradation of methyl orange azo dye. Phys B 445:48–55

Chen Q, Zhang ZJ (1998) Size-dependent superparamagnetic properties of $MgFe_2O_4$ spinel ferrite nanocrystallites. Appl Phys Lett 73:3156–3158

Chen D, Zhang Y, Tu C (2012) Preparation of high saturation magnetic $MgFe_2O_4$ nanoparticles by microwave-assisted ball milling. Mater Lett 82:10–12

Cullity BD (1956) Elements of X-ray diffraction. Addison-Wesley Publishing Company, Reading, p 259

Deraz NM, Shaban S (2009) Optimization of catalytic, surface and magnetic properties of nanocrystalline manganese ferrite. J Anal Appl Pyrolysis 86:173–179

Ferk G, Drofenik M, Lisjak D, Hamler A, Jagličić Z, Makove D (2014) Synthesis and characterization of $Mg_{1+x}Fe_{2-2x}Ti_xO_4$ nanoparticles with an adjustable Curie point. J Magn Magn Mater 350:124–128

Giannakopoulou T, Kompotiatis L, Kontogeorgakos A, Kordas G (2002) Microwave behavior of ferrites prepared via sol–gel method. J Magn Magn Mater 246:360–365

Hemeda OM, Mostafa NY, Abd Elkader OH, Ahmed MA (2014) Solubility limits in Mn–Mg ferrites system under hydrothermal conditions. J Magn Magn Mater 364:39–46

Hilpert S (1909) Correspondence as to Structure and Origin in Magnetic properties of Ferrite and Iron Oxide. Ber Deutsch Chem Ges 42:2248–2261

Kim DK, Zhang Y, Voit W, Rao KV, Muhammed M (2001) Synthesis and characterization of surfactant-coated superparamagnetic monodispersed iron oxide nanoparticles. J Magn Magn Mater 225:30–36

Koseoglu Y (2013) Structural, magnetic, electrical and dielectric properties of $Mn_xNi_{1-x}Fe_2O_4$ spinel nanoferrites prepared by PEG assisted hydrothermal method. J Ceram Int 39:4221–4230

Kotnala RK, Shah J, Singh B, Kishan H, Singh S, Dhawan SK, Sengupta A (2008) Humidity response of Li-substituted magnesium ferrite. J Sens Actuators B 129:909–914

Kotnala RK, Shah J, Mathpal MC, Gupta D, Purohit LP, Kishan H (2009) Role of modified active surface sites of magnesium ferrite for humidity sensing. J Optoelectron Adv Mater 11:296–301

Kotnala RK, Abdullah Dar M, Verma V, Singh AP, Siddiqui WA (2010) Minimizing of power loss in Li–Cd ferrite by nickel substitution for power applications. J Magn Magn Mater 322(22):3714–3719

Labde BK, Sable MC, Shamkuwar NR (2003) Structural and infra-red studies of $Ni_{1+x}Pb_xFe_{2-2x}O_4$ system. J Mater Lett 57(11):1651–1655

Liu C, Zhang ZJ (2001) Size-dependent superparamagnetic properties of Mn spinel ferrite nanoparticles synthesized from reverse micelles. J Chem Mater 13:2092–2096

Liu J, Li F, Evans DG, Duan X (2003) Stoichiometric synthesis of a pure ferrite from a tailored layered double hydroxide (hydrotalcite-like) precursor. Chem Commun 4:542–543

Mahmood A, Warsi MF, Ashiq MN, Ishaq MN (2013) Substitution of La and Fe with Dy and Mn in multiferroic $La_{1-x}Dy_xFe_{1-y}Mn_yO_3$ nanocrystallites. J Magn Magn Mater 327:64–70

Manikandan A, Vijaya JJ, Kennedy LJ, Bououdina M (2013) Structural, optical and magnetic properties of $Zn_{1-x}Cu_xFe_2O_4$ nanoparticles prepared by microwave combustion method. J Mol Struct 1035:332–340

Mansour SF (2011) Structural and magnetic investigations of sub-nano Mn–Mg ferrite prepared by wet method. J Magn Magn Mater 323:1735–1740

Modi KB, Shah SJ, Pujara NB, Pathak TK, Vasoya NH, Jhala IG (2013) Infrared spectral evolution, elastic, optical and thermodynamic properties study on mechanically milled $Ni_{0.5}Zn_{0.5}Fe_{2-}O_4$ spinel ferrite. J Mol Struct 1049:250–262

Nakagomi F, da Silva SW, Garg VK, Oliveira AC, Morais PC, Franco A Jr (2009) Influence of the Mg-content on the cation distribution in cubic $Mg_xFe_{3-x}O_4$ nanoparticles. J Solid State Chem 182:2423–2429

Naseri MG, Saion EB, Ahangar HA, Hashim M, Shaari AH (2011) Synthesis and characterization of manganese ferrite nanoparticles by thermal treatment method. J Magn Magn Mater 323:1745–1749

Néel L (1950) Propriétés magnétiques des ferrites: ferrimagnétisme et antiferromagnétisme. Ann De Phys 3(2):137–198

Pradeep A, Priyadarshini P, Chandrasekaran G (2011) Structural, magnetic and electrical properties of nanocrystalline zinc ferrite. J Alloys Compd 509:3917–3923

Rane KS, Verenkar VMS, Sawant PY (2001) Dielectric behaviour of $MgFe_2O_4$ prepared from chemically beneficiated iron ore rejects. Bull Mater Sci 24:323–330

Roduner E (2006) Size matters: why nanomaterials are different. J Chem Soc Rev 35:583–592

Srivastava M, Chaubey S, Ojha AK (2009) Investigation on size dependent structural and magnetic behavior of nickel ferrite nanoparticles prepared by sol–gel and hydrothermal methods. Mater Chem Phys 118:174–180

Stoner EC, Wohlfarth EP (1948) A mechanism of magnetic hystersis in hetrogeneous alloys. Philos Trans R Soc Lond Ser A 240:599. Reprinted by IEEE Trans Magn 27:3475 (1991)

Thankachan S, Jacob BP, Xavier S, Mohammed EM (2013) Effect of samarium substitution on structural and magnetic properties of magnesium ferrite nanoparticles. J Magn Magn Mater 348:140–145

Toledo JA, Valenzuela MA, Bosch P (2000) Effect of Al^{3+} introduction into hydrothermally prepared $ZnFe_2O_4$. Appl Catal A 198:235–245

Waldron RD (1955) Infrared spectra of ferrites. Phys Rev 99:1727–1735

Ye H, Jackman RB, Hing P (2003) Spectroscopic impedance study of nanocrystalline diamond films. J Appl Phys 94:7878–7882

Zhang Lei, He Yiming, Ying Wu, Tinghua Wu (2011) Photocatalytic degradation of RhB over $MgFe_2O_4/TiO_2$ composite materials. J Mater Sci Eng B 176:1497–1504